Plasma Sci. Technol. **20** (2018) 035404 (9pp) https://doi.org/10.1088/2058-6272/aaa357

Investigation on discharge characteristics of a coaxial dielectric barrier discharge reactor driven by AC and ns power sources

Qian WANG (王乾), **Feng LIU** (刘峰), **Chuanrun MIAO** (苗传润), **Bing YAN** (严冰) **and Zhi FANG** (方志)

College of Electrical Engineering and Control Science, Nanjing Tech University, Nanjing 211816, People's Republic of China

E-mail: myfz@263.net

Received 11 October 2017, revised 14 December 2017
Accepted for publication 19 December 2017
Published 1 February 2018

Abstract

A coaxial dielectric barrier discharge (DBD) reactor with double layer dielectric barriers has been developed for exhaust gas treatment and excited either by AC power or nanosecond (ns) pulse to generate atmospheric pressure plasma. The comparative study on the discharge characteristics of the discharge uniformity, power deposition, energy efficiency, and operation temperature between AC and ns pulsed coaxial DBD is carried out in terms of optical and electrical characteristics and operation temperature for optimizing the coaxial DBD reactor performance. The voltages across the air gap and dielectric layer and the conduction and displacement currents are extracted from the applied voltages and measured currents of AC and ns pulsed coaxial DBDs for the calculation of the power depositions and energy efficiencies through an equivalent electrical model. The discharge uniformity and operating temperature of the coaxial DBD reactor are monitored and analyzed by optical images and infrared camera. A heat conduction model is used to calculate the temperature of the internal quartz tube. It is found that the ns pulsed coaxial DBD has a much higher instantaneous power deposition in plasma, a lower total power consumption, and a higher energy efficiency compared with that excited by AC power and is more homogeneous and stable. The temperature of the outside wall of the AC and ns pulse excited coaxial DBD reaches 158 °C and 64.3 °C after 900 s operation, respectively. The experimental results on the comparison of the discharge characteristics of coaxial DBDs excited by different powers are significant for understanding of the mechanism of DBDs, reducing energy loss, and optimizing the performance of coaxial DBD in industrial applications.

Keywords: coaxial dielectric barrier discharge, discharge characteristics, nanosecond pulse, operation temperature

(Some figures may appear in colour only in the online journal)

1. Introduction

Dielectric barrier discharge (DBD) is a type of gas discharge, which can produce high electron temperature and low gas temperature non-thermal plasma at atmospheric pressure. In a DBD, at least one of the electrodes is covered by dielectric layer, which can limit the current and prevent the discharge transfer to arc discharge. DBD has the advantages of simple structure, uniform discharge, and moderate energy density. For over a century, it has been widely used in the fields of cleaning of flue gases [1–3], materials surface treatment [4, 5], medical sterilization [6, 7], ozone production [8, 9], and synthesis of fuels and chemicals [10, 11]. Coaxial DBDs' shape allows for gas flow between coaxial cylindrical electrodes in a manner that allows for the gas to be treated evenly. Therefore, it is suitable for large volume gas reactants treatment, such as removal of NO_x and SO_2 from flue gas [11, 12] and reformation of methane [13, 14].

Since DBDs have been traditionally driven by AC powers sources, there exists an extensive amount of studies on the discharge characteristics, electrode structures, and treatment effects of AC DBDs [11, 15–17]. It is found that the energy efficiency of AC DBD is low because most of the electrical energy goes into gas heating and there are a lot of filaments in discharge regime, which may result in the local overheating of the reactor and the uneven treatment. With the development of pulse power technology, pulsed DBD has been actively studied and applied in various applications [18–21]. Relative to AC-driven DBDs, pulsed-driven DBDs improve the energy efficient of the system by using a fast rise time of voltage pulse brings more energy into the energetic electrons generation, which play a critical role in plasma physicochemical processing, and the discharge uniformity is also improved dramatically [18, 22]. Zhang *et al* compared the discharge uniformity, average power consumption, and plasma gas temperatures of AC and nanosecond (ns) pulsed DBD and found that the ns pulsed DBD had a better discharge uniformity, a lower average power consumption, and a lower operation temperature than AC DBD under the same applied voltage [23]. Kettlitz M *et al* reported the spatial and temporal structure of the breakdown process of AC and μs pulsed dielectric barrier micro-discharges and the results showed microsecond (μs) DBD had lower streamer velocities than AC DBD [24]. Williamson *et al* investigated the ozone generation rate of DBD excited by short-pulse and high voltage AC excitation and found that the short-pulse DBD had higher electron density and ozone generation rate than those of the AC DBD under the same power [25]. These findings demonstrate that the pulsed DBD has advantages on energy efficiency, discharge uniformity, and the treatment effects compared with the AC DBD. However, there has little work been done with the comprehensive comparison on the coaxial DBD excited by AC and ns power supplies in the discharge characteristics including discharge uniformity, discharge power, energy efficiency, and operating temperature, which are critical important for the coaxial DBD practical applications in industrial field.

In this paper, the influence of AC and ns pulse power supplies on the discharge characteristics of coaxial DBD are comprehensively studied by electrical and optical diagnosis and temperature measurements. The energy efficiency, the average power consumption of the air gap, and reactor heat loss rate of AC and ns pulse excited coaxial DBD are calculated and compared by equivalent circuit model and heat conduction model analysis.

2. Experimental setup

The experimental setup is illustrated schematically in figure 1(a). The coaxial DBD can be excited by AC and ns pulse power supplies, respectively. The AC power frequency varies from 5 to 20 kHz and the peak output voltage is ranged from 0 to 25 kV. The AC power supply is based on self-oscillating technology and the central oscillating frequency is 9.5 kHz. At the central oscillating frequency, the AC power supply has high power factor and sinusoidal voltage waveform output. Then, the frequency of the AC power supply is fixed at 9.5 kHz during experiment for best discharge performance. The ns pulse power supply can provide adjustable high-voltage pulses of up to 30 kV with a rising time of 80 ns and a pulse width of 250 ns. The pulse repetition frequency (PRF) of ns pulse power supply varies from 0 to 1 kHz and is fixed at 1 kHz during experiment. The experiment is carried out in open air under one atmospheric pressure with 20 °C room temperature and 20% humidity. A cross-sectional view of the coaxial DBD reactor is shown in figure 1(b). It includes inter electrode, outer electrode, and internal and external dielectric barrier layers. Reactor is built up by two coaxial quartz tubes with a 2.5 mm gas gap and quartz tubes serve as dielectric barrier layers between the inner and outer electrodes. The external quartz tube has a thickness of 2.5 mm, a length of 360 mm, and an outer diameter of 25 mm. While the internal quartz tube has a thickness of 1.2 mm, a length of 355 mm and an outer diameter of 15 mm. The outer surface of the external quartz tube is wrapped by a stainless steel mesh with a length of 200 mm and is connected with the power supply output as the high-voltage electrode. The inter electrode in the middle of the internal quartz tube is a 1 mm diameter copper wire connected with ground as the grounded electrode. The aluminum powder is filled the space between the inner electrode and the internal quartz tube for uniform heat transfer and reducing partial discharge.

The applied voltage and the discharge current are measured with a 1000:1 high-voltage probe (Tektronix, P6015A) and a current coil (Pearson Electronics Inc., 2877), respectively. A 2200 pF reference capacitor, C_m, is inserted in the circuit to estimate the voltage across the dielectric barrier and the voltage on C_m is measured using a 200:1 differential probe (Sapphir, LDP-6002). The voltage and current waveforms are recorded by a digital oscilloscope (Tektronix, TDS-3054c). The discharge image is recorded by a digital camera (Canon, EOS6D) with an exposure time of 1/25 s. The temperature of the external quartz tube is measured using an infrared (IR) camera (Testoterm, Testo875-1i) with a measurement range of 0 °C–350 °C.

3. Electrical analysis and modeling

For a coaxial DBD, the applied voltage, U_t, is the sum of the voltage across the gap, U_g, and the voltage across the dielectric barrier, U_d, and the measured current, I_t, is composed of the displacement current, I_d, and the conduction current, I_g. The U_g and I_g are important to analyze the ignition and extinguish processes of DBD and calculate the power used for plasma generation. To separate the U_t and I_g, an equivalent circuit of the coaxial DBD reactor is used and is shown as figure 2 [26, 27]. C_d represents the equivalent capacitance of both dielectric layers, C_g represents the equivalent capacitance of air gap, and C_{eq} is the total equivalent capacitance of the DBD configuration. In addition, a reference capacitor, C_m, is used for calculating U_d and the value of C_m should be far larger than that of C_{eq}. Then, it can avoid the influence of C_m in the discharge.

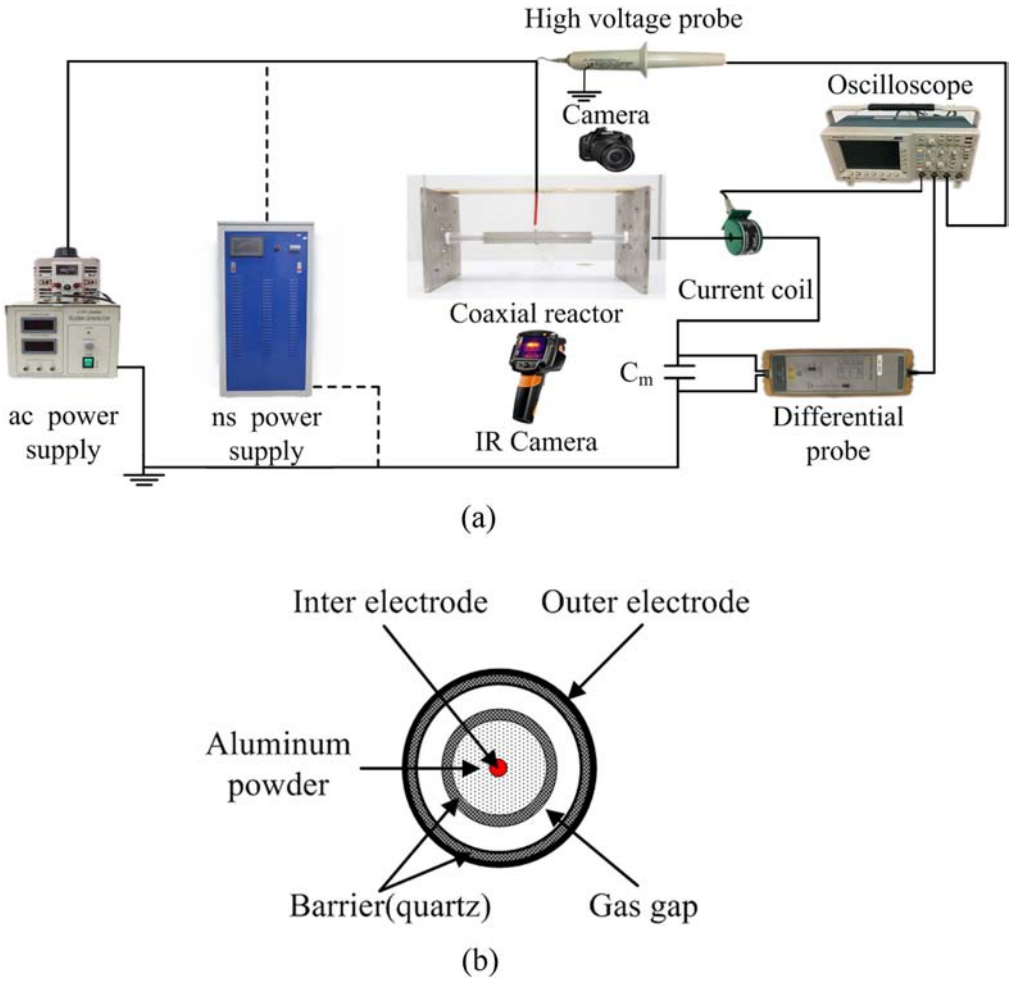

Figure 1. The schematic of the coaxial DBD experimental setup (a) and the cross-sectional view of the coaxial DBD reactor (b).

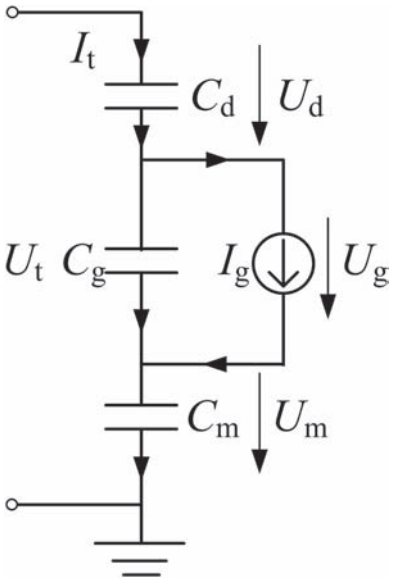

Figure 2. The equivalent electrical circuit of the coaxial DBD reactor.

When the discharge is not on, I_d is equal to the measured current I_t [28] and C_{eq} can be obtained with equation (1) [19]:

$$I_d = C_{eq}\frac{dU_t}{dt}. \quad (1)$$

Figures 3(a) and (b) show the measured currents I_t without discharge, which should be pure displacement current, and the fitting curves I_d from equation (1) of AC and ns pulsed coaxial DBD. The I_d is obtained by the product of $\frac{dU_t}{dt}$ and an amplification coefficient as shown in equation (1). The amplification coefficient is selected such that the calculated I_d waveform fitting well with the measured currents I_t without discharge. Then, the obtained amplification coefficient is equal to C_{eq}. According to the above method, the equivalent capacitances of AC and ns pulsed coaxial DBDs are obtained as 37 pF and 50 pF, respectively. The difference of the equivalent capacitances of the AC and ns pulsed coaxial DBDs is because the charge distribution on the dielectric barrier in ns pulse excited coaxial DBD reactor is more uniform than that in AC excited coaxial DBD reactor.

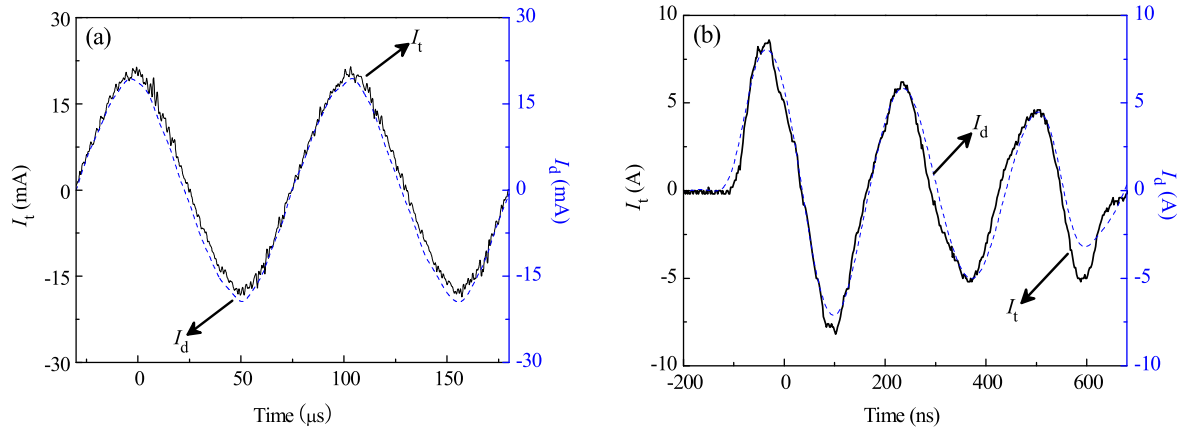

Figure 3. The measured current and the calculated displacement current without discharge: (a) AC coaxial DBD, (b) ns pulsed coaxial DBD.

When the applied voltage is increased and the discharge is on, the obtained C_{eq} can still be used to represent the equivalent capacitance for it does not change much with the discharge conditions [29]. When the discharge on, the discharge current through the gap, I_g, can be obtained by equation (2) with a measured I_t and a calculated I_d by equation (1):

$$I_g = I_t - I_d. \tag{2}$$

U_d, is proportional to U_m for both capacitive loads according to the equivalent circuit. Then, U_d can be estimated by carefully selecting a coefficient k in equation (3). For AC DBD, the coefficient k is the inverse of the capacitances of C_{eq} and C_m. For ns DBD, the constant, k, is selected such that U_g could be near zero when the discharge is extinguished [30].

$$U_d = kU_m. \tag{3}$$

U_g can be obtained by equation (4):

$$U_g = U_t - U_d. \tag{4}$$

According to the above equations, the instantaneous total power input, P_t, can be calculated as following:

$$P_t = U_t \times I_t. \tag{5}$$

The instantaneous power consumption of air gap, P_g, and the instantaneous power consumption of dielectric layer, P_d, can be obtained from the equations (6) and (7).

$$P_g = U_g \times I_g, \tag{6}$$

$$P_d = P_t - P_g. \tag{7}$$

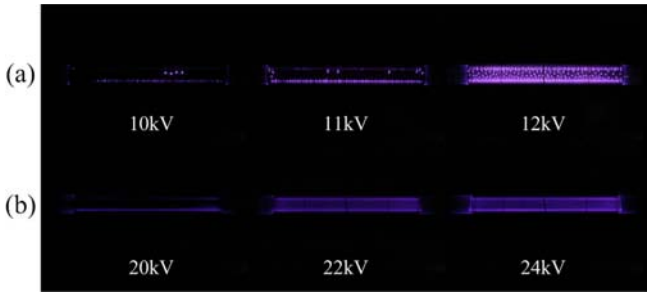

Figure 4. The discharge images of (a) AC coaxial DBD and (b) ns pulsed coaxial DBD at various applied voltages.

The average power consumption of the coaxial DBD reactor, $\overline{P_t}$, the average power consumption of air gap, $\overline{P_g}$, and the average power consumption of dielectric layer, $\overline{P_d}$ can be expressed as follows:

$$\overline{P_t} = \frac{1}{T}\int_0^T P_t \mathrm{d}t, \tag{8}$$

$$\overline{P_g} = \frac{1}{T}\int_0^T P_g \mathrm{d}t, \tag{9}$$

$$\overline{P_d} = \overline{P_t} - \overline{P_g}. \tag{10}$$

The energy efficiency of the coaxial DBD is calculated as:

$$\eta = \frac{\overline{P_g}}{\overline{P_t}} \times 100\%. \tag{11}$$

4. Experimental results

4.1. Discharge uniformity

The discharge images of the coaxial DBD excited by AC and ns pulse power sources at various applied voltages are shown in figures 4(a) and (b), respectively. The frequency has effect on

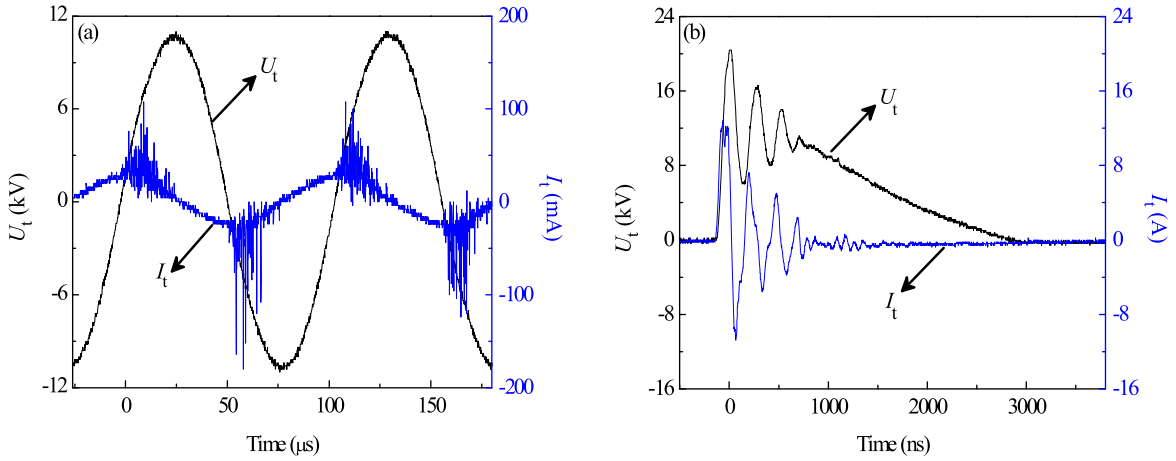

Figure 5. The typical voltage and current waveforms of (a) AC coaxial DBD and (b) ns pulsed coaxial DBD.

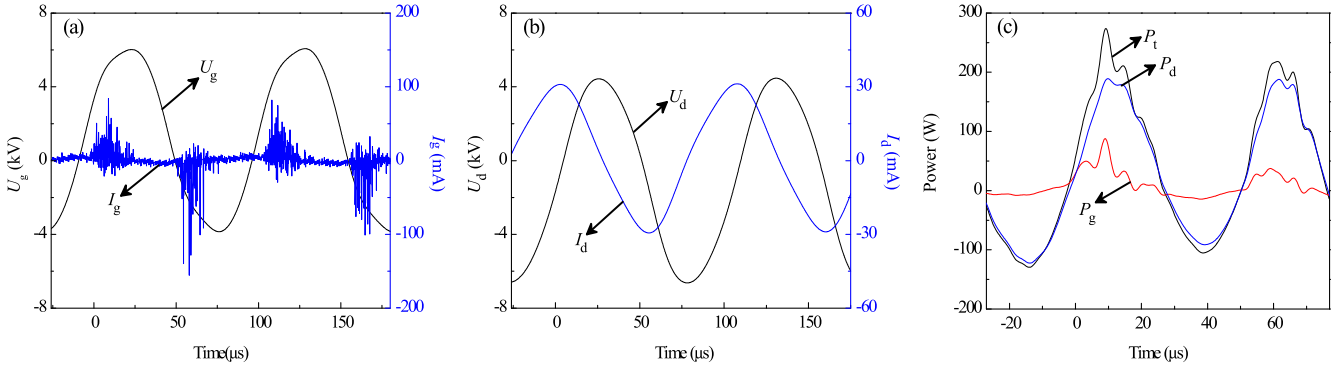

Figure 6. The calculated U_g and I_g (a), the calculated U_d and I_d (b), and the corresponding P_t, P_d, and P_g (c) with 11 kV and 9.5 kHz.

the intensity of the discharge. The intensity of the discharge images is higher with a higher frequency but the variation of the frequency has little effect on the discharge uniformity. It is clearly shown that the ns pulsed coaxial DBD is more homogeneous than the AC coaxial DBD. In figure 4(a), it can be seen that there are a lot of filaments in the AC DBD air gap. At a lower applied voltage, the filaments are weak and only a few bright spots can be observed at the inner and outside walls of dielectric barrier tubes. With the increase of the applied voltage, there are more filaments in the air gap and more bright spots all over the walls of dielectric barrier tubes.

Figure 4(b) shows the discharge images of the ns pulsed coaxial DBD is diffuse and there is no filament observed. When the peak voltage is low, the plasma is initiated on localized areas such as the edge of the high-voltage electrode and the discharge in the middle zone is weak. With the increase of the applied voltage, the discharge is more uniform in the air gap and is illumined the whole space between the outer electrode and inner electrode. The ns pulsed discharge has a very short voltage rising time and a short voltage duration, which prevent the glow to arc transition. Therefore, from the optical images, the ns pulsed coaxial DBD is more uniform than the AC DBD.

4.2. Electrical characteristics

Figures 5(a) and (b) show the voltage–current waveforms of the AC coaxial DBD at 11 kV peak voltage and ns pulsed coaxial DBD at 21 kV peak voltage, respectively. It can be seen in figure 5(a) that there are many filaments in both the positive and negative half cycles of the measured current, which indicates that the discharge is in filamentary mode. The peak value of the ns pulsed coaxial DBD current in figure 5(b) is much higher than that of the AC coaxial DBD and the current only contains a few peaks, which is corresponding to the conduction current and displacement current.

With the applied voltage and measured current of figure 5(a) and equations (1)–(7), the discharge parameters, U_g, I_g, U_d, I_d, P_t, P_g, and P_d of AC coaxial DBD at 11 kV peak voltage and 9.5 kHz frequency are obtained and shown in figure 6. It can be seen that the peak values of P_t is about 280 W, P_d is about 190 W and P_g is about 90 W, which means most of the power deposited into the dielectric barrier other than plasma generation.

With the applied voltage and measured current of figure 5(b), U_g, I_g, U_d, I_d, P_t, P_g, and P_d of ns pulsed coaxial DBD at 21 kV peak voltage and 1 kHz PRF are obtained and shown in figure 7. It can be seen that the peak values of P_t is

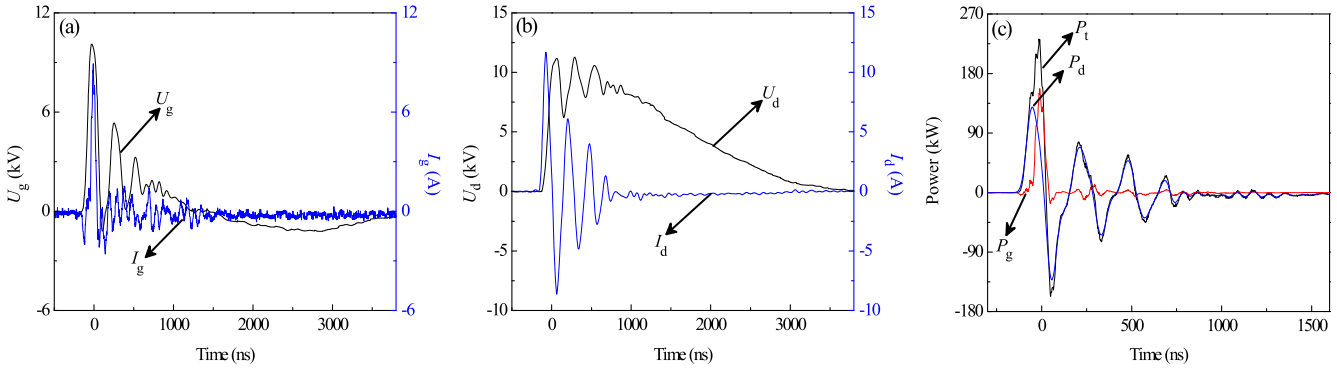

Figure 7. The calculated U_g and I_g (a), the calculated U_d and I_d (b), and the corresponding P_t, P_d, and P_g (c) with 21 kV and 1 kHz.

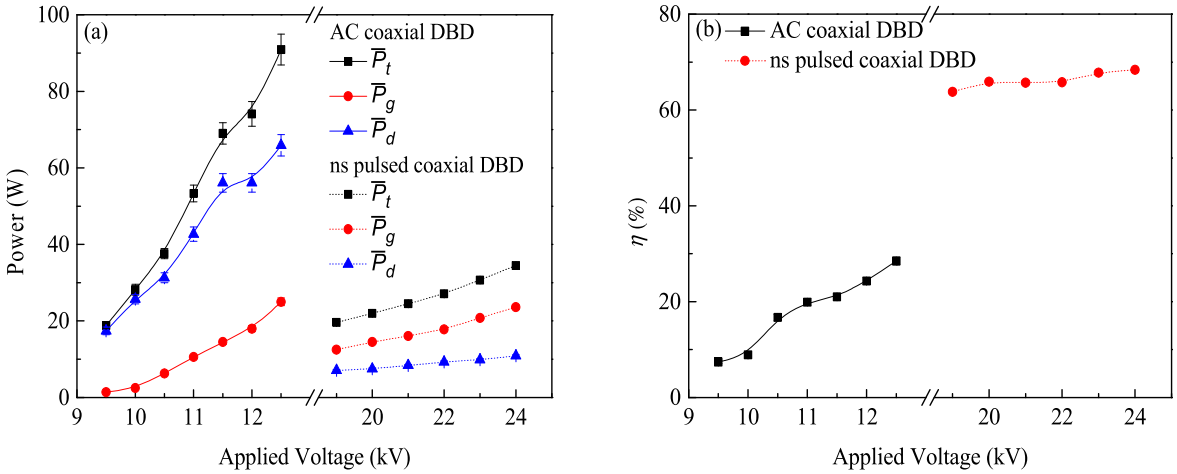

Figure 8. The variations of $\overline{P_t}$, $\overline{P_g}$, $\overline{P_d}$ and η of (a) AC coaxial DBD and (b) ns pulsed coaxial DBD at various applied voltages.

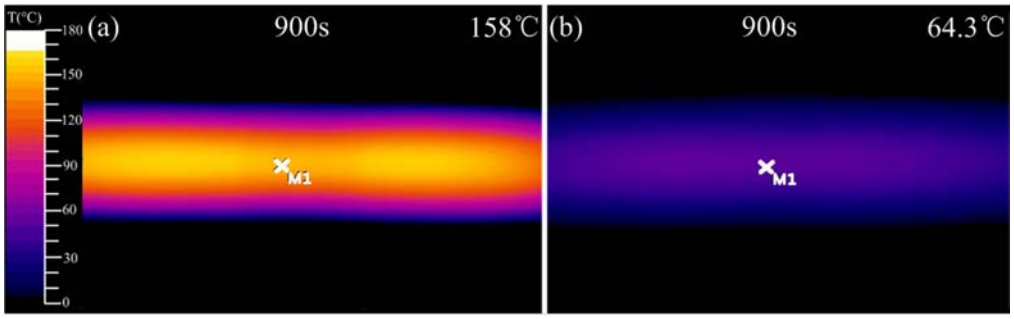

Figure 9. The 2D temperature profiles of the outside wall of (a) AC coaxial DBD and (b) ns pulsed coaxial DBD.

about 250 kW, P_d is about 120 kW and P_g is about 160 kW, which are much higher than those of the AC coaxial DBD. It means that the ns pulsed coaxial DBD has a much higher power deposited into air gap than the AC coaxial DBD to generate plasma.

To further investigate the discharge characteristics of the coaxial DBD excited by AC and ns pulse power sources, η, $\overline{P_t}$, $\overline{P_g}$ and $\overline{P_d}$ of AC and ns pulsed coaxial DBD at their operation voltages from breakdown voltage to unstable voltage (AC coaxial DBD: 9.5–12.5 kV; ns pulsed coaxial DBD: 19–24 kV) are plotted in figure 8. The breakdown voltage of the ns pulsed DBD is much higher than that of the AC coaxial DBD because it has a much faster voltage rising time. It can be seen that $\overline{P_t}$, $\overline{P_g}$ and $\overline{P_d}$ obtained from equations (8)–(10) increase with the increase of the applied voltage. η obtained from equation (11) also shows an increased trend with the increase of applied voltage for both AC and ns pulsed DBDs. For AC coaxial DBD, $\overline{P_t}$ and $\overline{P_g}$ are in the ranges of about 18–95 W and 2–25 W over the studied voltages. For ns pulsed coaxial DBD, $\overline{P_t}$ and $\overline{P_g}$ are in the ranges of about 18–35 W and 11–23 W over the studied voltages. The ns pulsed coaxial DBD has a much higher η compared with that of the AC coaxial DBD, which means most of the energy goes into plasma generation. The maximum values of the η of the ns

Table 1. Parameters of the different materials of the coaxial DBD reactor.

	Aluminum powder	Internal quartz tube	External quartz tube	Air
V (m^3)	2.5×10^{-5}	1×10^{-5}	3.5×10^{-5}	2.7×10^{-5}
ρ ($kg\ m^{-3}$)	2700	2650	2650	1.29
C_P ($J\ kg^{-1}\ k^{-1}$)	880	800	800	1400
mC_P ($J\ k^{-1}$)	59.4	21.2	74.2	0.05

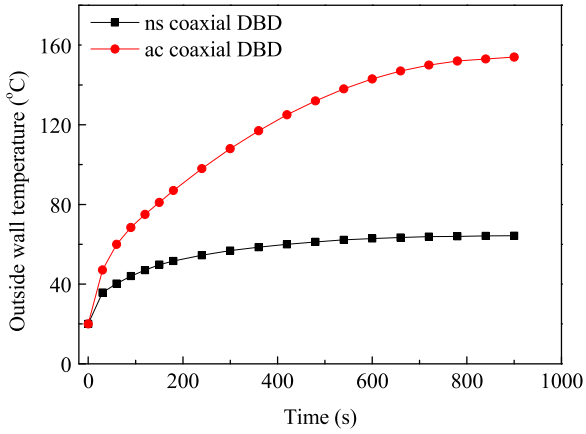

Figure 10. The variations of the outside wall temperatures of AC and ns pulsed coaxial DBD reactor as a function of operating time.

pulsed coaxial DBD is 68.4%, while the AC coaxial DBD is only 28.5% in the studied applied voltages.

4.3. Operating temperature

In practical applications, the operation temperature of the coaxial DBD reactor is a key factor for the selection of dielectric barrier material, reactor lifetime, heat loss, and treatment effects. To extend the coaxial DBD reactor lifetime and reduce the cost of the reactor, the operation temperature should remain at a low level. The two-dimensional temperature profiles of the outside wall temperature of the coaxial DBD reactor driven by AC and ns pulse power supplies after 900 s operation are obtained by placing the IR camera perpendicular to the axis of tube and are shown in figures 9(a) and (b), respectively. The discharge conditions are selected with the most power output, which are close to the practical operation conditions. The peak voltage of the AC coaxial DBD is 12.5 kV and the frequency is 9.5 kHz and the peak voltage of the ns pulsed coaxial DBD is 24 kV and the PRF is 1 kHz. The highest temperatures of the outside wall (marked on figure 9) of AC and ns pulsed coaxial DBD reactor are 158.0 °C and 64.3 °C, respectively.

Figure 10 shows the variation of the outside wall temperatures of the AC and ns pulsed coaxial DBD reactor with the operation time. It can be seen that the temperatures rise gradually with the operation time and reach thermal balance with a time about 900 s. Moreover, the temperature of the ns pulsed coaxial DBD reactor is much lower than that of the AC coaxial DBD reactor. It is because there is more energy consumed on the dielectric layer of the AC coaxial DBD reactor other than the ns pulsed coaxial DBD reactor within the same operation time.

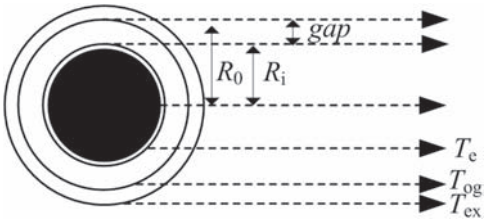

Figure 11. The sectional view of DBD reactor for thermal analysis.

5. Discussion

To further analyze the heat loss of the coaxial DBD reactor excited by AC and ns pulse and provide guidance for practical application, the thermal balance analysis is carried out with a heat conduction model [31] as follows. The sectional view of the coaxial DBD reactor for thermal analysis is shown in figure 11, where R_i is the inner radius of the external quartz tube, R_o, is the outer radius of the internal quartz tube, T_e, T_{og}, and T_{ex} are the temperatures at the surface of the internal quartz tube, inner surface of the external quartz tube, and the outer electrode. It assumes that part of the total input power is used to produce the plasma and the rest is consumed by the dielectric layer as heat loss.

The heat capacity, C_i, of each part of the reactor can be obtained by the following expression [32].

$$C_i = m_i \cdot C_{Pi} \tag{12}$$

where m_i and C_{Pi} are respectively the mass and the specific heat of aluminum powder, internal quartz tube, external quartz tube, and gas. The volume, density, specific heat, and heat capacity of aluminum powder, internal quartz tube, external quartz tube, and gas are given in table 1. The total heat capacity is 154.85 $J\ K^{-1}$.

Where V is the volume of each part, ρ is the density, C_{Pi} is specific heat capacity of each part, and m_iC_{Pi} is the heat capacity. The energy consumption on the dielectric layer converts to heat and transfers to the environment. When the heat produced in the coaxial DBD reactor is equal to the heat released, the temperature of the coaxial DBD reactor reaches a balance state. The heat conduction model of the coaxial DBD is expressed as follows:

$$P_e - \Delta P_e = P_{e1}, \tag{13}$$

Table 2. The heat parameters of AC and ns pulsed coaxial DBD reactor.

	W_e (J)	$\overline{P_t}$ (W)	ΔP_{og} (W)	T_{og} (°C)	T_e (°C)	η_l (%)
AC coaxial DBD reactor	8395.2	90.9	65.9	158	461	72.5
ns pulsed coaxial DBD reactor	1992.8	34.5	10.9	64.3	114	31.6

$$P_{og} + \Delta P_e - \Delta P_{og} = P_{og1}, \tag{14}$$

$$P_e + P_{og} = \overline{P_d}, \tag{15}$$

$$\Delta P_{og} \approx \frac{T_e - T_{ex}}{\frac{1}{4\pi\lambda L}\ln\left(\frac{R_0}{R_i}\right)}, \tag{16}$$

where ΔP_{og} is the heat loss that the reactor releases into the environment. It can be calculated by the equation (16) [31]. P_e and P_{og} are the instantaneous heat consumption of the internal and the external quartz tubes. ΔP_e is the heat released by the internal quartz tube. P_{e1} and P_{og1} are the total heat consumption of the internal and the external quartz tubes and L is the length of the outer electrode. According to a simple heat conduction model developed by Sadat and Dubus [31], we can calculate the radial variation of temperature by the following expression:

$$T = T_e - \frac{A}{2\lambda}\left[\ln\left(\frac{r}{R_i}\right)\right]^2, \tag{17}$$

where T is the radial temperature, A is a constant, λ is the thermal conductivity (air: 0.025 W m^{-1} °C^{-1}), and r is radius. Because the outer electrode is very thin, the temperature at the outer surface, T_{ex}, can be assumed to be equal to T_{og}. When the steady state is reached, the heat absorbed by the reactor is equal to the heat released by the external quartz tube, leads to the following solution:

$$\Delta P_{og} = \overline{P_d}. \tag{18}$$

The temperature at the surface of the inter electrode can be calculated by the equations (16) and (18). During the experiment, the temperature is 20 °C. The heat of the internal quartz tube, W_e, can be calculated by the equation (19).

$$W_e = m \cdot C_p \times (T_e - 20). \tag{19}$$

The heat loss rate can be calculated by the following definition.

$$\eta_l = \frac{\Delta P_{og}}{\overline{P_t}}. \tag{20}$$

The calculated heat of the internal quartz tube, the average power consumption of the DBD reactor, the heat loss into the environment, the temperature at the inner surface of the external quartz tube (T_{og}) and the inter electrode (T_e), and the calculated heat loss rate are summarized in table 2. It can be seen that the temperatures of the internal and the external quartz tubes in the AC coaxial DBD reactor are higher than that in the ns pulsed coaxial DBD reactor, which result in most of energy of the AC coaxial DBD is used for heating and the ns pulsed coaxial DBD has a much higher energy efficiency than the AC coaxial DBD.

6. Conclusions

The discharge characteristics of coaxial DBD driven by high voltage AC and ns pulse power supply are obtained and compared including the discharge uniformity, average power consumption, energy efficiency, and operating temperature. From the observation of optical images, the ns pulsed coaxial DBD is more uniform than the AC coaxial DBD, which can improve the treatment effects and avoid the overheating of the reactor. The operating temperatures of coaxial DBD reactors excited AC and ns pulse are recorded by IR camera that the ns pulsed coaxial DBD has a much lower operation temperature, 64.3 °C, than AC coaxial DBD, 158 °C, after 900 s operation. The lower operating temperature is more suitable for long time operation in the large-scale industrial applications. An equivalent electrical model and a heat conduction model are used to analyze the power consumption, the energy efficiency, and the heat loss of reactor. It is found that the ns pulsed coaxial DBD has a much higher instantaneous power deposition in air gap than AC coaxial DBD. The energy efficiency of the ns pulsed coaxial DBD can reach 68.4%. While, the energy efficiency of the AC coaxial DBD is below 30%. Most of the energy in AC coaxial DBD is used to heat the reactor and the temperature of the inner dielectric barrier of AC coaxial DBD is also much higher than that of ns pulsed coaxial DBD. The findings are important to understand the discharge mechanisms of AC and ns pulsed coaxial DBD. The results also can provide important experimental references to control the discharge properties, optimize the reactor design, and improve the performance of coaxial DBD reactors in industrial applications.

Acknowledgments

This work is supported by National Natural Science Foundation of China (Nos. 51777091 and 51677083).

References

[1] Wang T *et al* 2012 *Plasma Chem. Plasma Process.* **32** 1189
[2] Liang W J *et al* 2011 *J. Electrostat.* **69** 206
[3] Chen J and Xie Z M 2013 *J. Hazard. Mater.* **261** 38
[4] Shao T *et al* 2014 *Appl. Phys. Lett.* **105** 071607
[5] Yang G Q, Zhang G J and Zhang W Y 2011 *Plasma Sci. Technol.* **13** 617
[6] Mastanaiah N *et al* 2013 *Plasma Process. Polym.* **10** 1120
[7] Eto H *et al* 2008 *Plasma Process. Polym.* **5** 269
[8] Sung Y M and Sakoda T 2005 *Surf. Coat. Technol.* **197** 148
[9] Fang Z *et al* 2008 *J. Electrostat.* **66** 421
[10] Tu X *et al* 2011 *J. Phys. D: Appl. Phys.* **44** 274007

[11] Tu X and Whitehead J C 2012 *Appl. Catal.* B **125** 439
[12] Peters F *et al* 2016 *Plasma Sci. Technol.* **18** 406
[13] Ma H B *et al* 2002 *Plasma Chem. Plasma Process.* **22** 239
[14] Kolb T *et al* 2012 *Plasma Chem. Plasma Process.* **32** 1139
[15] Dou B J *et al* 2013 *J. Electrostat.* **71** 939
[16] De Geyter N *et al* 2007 *Surf. Coat. Technol.* **201** 7066
[17] Wang C Q, Zhang G X and Wang X X 2012 *Vacuum* **86** 960
[18] Yang D Z *et al* 2013 *Appl. Phys. Lett.* **102** 194102
[19] Shao T *et al* 2008 *J. Phys. D: Appl. Phys.* **41** 215203
[20] Shao T *et al* 2011 *Plasma Sci. Technol.* **13** 591
[21] Zhang L *et al* 2017 *Plasma Sci. Technol.* **19** 064006
[22] Jiang H *et al* 2011 *IEEE Trans. Plasma Sci.* **39** 2076
[23] Zhang S *et al* 2013 *J. Appl. Phys.* **114** 163301
[24] Kettlitz M *et al* 2013 *Plasma Sources Sci. Technol.* **22** 025003
[25] Williamson J M *et al* 2006 *J. Phys. D: Appl. Phys.* **39** 4400
[26] Liu S H and Neiger M 2001 *J. Phys. D: Appl. Phys.* **34** 1632
[27] Liu S H and Neiger M 2003 *J. Phys. D: Appl. Phys.* **36** 3144
[28] Zhang C *et al* 2013 *IEEE Trans. Dielectr. Electr. Insul.* **20** 1304
[29] Pipa A V *et al* 2012 *Rev. Sci. Instrum.* **83** 075111
[30] Liu F, Huang G and Ganguly B 2010 *Plasma Sources Sci. Technol.* **19** 045017
[31] Sadat H *et al* 2009 *Appl. Therm. Eng.* **29** 1259
[32] Sadat H *et al* 2010 *J. Electrostat.* **68** 27